



DOI: 10.34910/MCE.109.5

The shear behavior of Anchored CFRP Strengthened RC beams

R. Al-Rousan 

Jordan University of Science and Technology, Irbid, Jordan

E-mail: rzalrousan@just.edu.jo

Keywords: reinforced concrete, anchored, shear, flexural strength, fiber reinforced polymer, nonlinear, finite element analysis

Abstract. The primary objective of this paper is to study the effectiveness of anchorage on the performance of shear deficient beams externally strengthened with carbon fiber-reinforced polymers (CFRP) composites. The overall behavior of the tested beams loaded up to failure, the onset of the cracking, and crack development with increased load and ductility were described. The use of CFRP composites is an effective technique to enhance the shear capacity of reinforced concrete (RC) beams. The externally bonded CFRP can increase the shear capacity of the beam significantly making it 15–34 % more than that of the control beams, depending on the variables investigated. The use of CFRP composites is an effective technique to enhance the shear capacity of RC beams by using CFRP strips anchored into the tension side and from the top. Bonded anchorage of CFRP strips with width of 0.1h, 0.2h, and 0.3h to the beam resulted in a decrease in average interface bond stress and an increase in the effective strain of the FRP sheet at failure. This resulted in a higher shear capacity as compared with that of the U-wrapped beams without anchorage as well as helped delay or mitigate the sheet debonding from the concrete surface. Finally, an inclusive assessment of the NLFEA results is conducted using a large test database of well-known shear strength models.

1. Introduction

Premature debonding failure of reinforced concrete beams strengthened with externally bonded fiber reinforced polymers (FRP) is a frequent problem. Therefore, developing anchorage devices to enhance the composite action between the FRP sheets and the concrete beam is a big challenge to prevent the debonding of the FRP plates from a concrete beam. Mechanical anchorage is a useful method to prevent this mode of failure, therefore improving the performance of the conventional FRP-strengthening method. Knowledge of anchorage systems is limited and further experimental and numerical studies to understand their behavior are still necessary to optimize their performances.

Concrete structures (for example: buildings, bridge decks, girders, offshore structures, parking lots) are subject to damage because of: improper maintenance, steel corrosion, ageing, faulty design or construction, additional excessive loading such as heavy traffic, the seismic movements, and harsh environmental condition. Due to the old codes of design, or not complying with the new ones as in some countries, many structures are endangered, and need to be strengthened and/or rehabilitated [1]. It has been reported that 23 % of the concrete bridges in the USA are deficient or not in service [2]. Deficient structure can be repaired or demolished. However, the latter could cause damages, sometimes severe, to the adjacent structures, resulting in financial losses. Therefore, there is a need to find adequate techniques and materials to strengthen and/or repair such structures. The strengthening technique of bonding, externally, carbon-fiber reinforced polymer (CFRP) laminates has been widely adopted to repair, strengthen, and rehabilitate deficient or damaged structures [3–6]. The RC structures, commonly, fail or get defected in shear or flexure. Between these two, the deficiency in shear is much more serious because it occurs suddenly, without giving the element the chance to deal with the developed internal stresses. The

Al-Rousan, R. The shear behavior of Anchored CFRP Strengthened RC beams. Magazine of Civil Engineering. 2022. 109(1). Article No. 10905. DOI: 10.34910/MCE.109.5

© Al-Rousan R., 2022. Published by Peter the Great St. Petersburg Polytechnic University.



This work is licensed under a CC BY-NC 4.0

shear failure could be due to improper designing, reduction in shear reinforcement (RFT) that is caused by steel corrosion or overloading. The use of externally-bonded FRP material's efficiency to enhance the shear capacity [7–11] is governed, mainly, by its: tensile strength, the ratio of shear reinforcement, the used configuration. In addition, the FRP's efficiency is also affected by the inclination angle of shear cracks, the concrete's compressive strength, and the yield strength of both the shear reinforcement and steel bars, adding to its ratio of tensile reinforcement. Reinforcing RC structural elements with externally-bonded FRP has been the focus of many researches [12–14]; several analytical investigations have been carried out to study the strengthened RC beams' shear performance in terms of strengthening methods [15, 16], section shape [17, 18], design equations [19, 20].

The use of CFRP composites in rehabilitating structures can greatly reduce maintenance requirements, increase life safety and service life of concrete structures. So far, the majority of research and applications carried out, using CFRP as strengthening material, has been devoted to use for flexural strengthening. A reinforced concrete beam must be designed to develop its full flexural strength to insure a ductile flexural failure mode under extreme loading. Hence, a beam must have a safety margin against other types of failure that are more dangerous and less predictable than flexural failure. The use of external FRP strengthening to beams may be classified as flexural and shear strengthening. The shear failure of an RC beam is distinctly different from the flexural one in that the flexural is ductile in nature, whereas the shear one is brittle and catastrophic. When the RC beam is deficient in shear, or when its shear capacity is less than the flexural capacity after flexural strengthening, shear strengthening of the beam must be considered. It is critically important to examine the shear capacity of RC beams which are intended to be strengthened in flexure. However, only a few studies on the shear strengthening of RC T-beams with externally bonded FRPs are reported in the literature. Deniaud and Cheng [21] studied the interaction of concrete, steel stirrups, and external fiber-reinforced polymer (FRP) sheets in carrying shear loads in RC T-beams. Boushelham and Chaallal [22] investigated the effect of the shear length to the beam depth ratio, the CFRP ratio and the internal transverse steel reinforcement ratio on the shear behavior of RC T-beams. Boushelham and Chaallal [23] evaluated the effect of the different parameters on the shear performance of strengthened RC T-beams. In addition, they [24] investigated the shear resistance mechanisms in RC T-beams strengthened in shear with externally bonded FRP.

The interface between FRP and concrete is the most important part in the process of repairing or strengthening concrete structures. To obtain high efficiency of repaired or strengthened concrete structures, we must provide sufficient bonding strength between the concrete surface and the FRP to ensure a good transmission between the concrete surface and the FRP since many failure modes occur due to debonding between the concrete surface and the FRP materials. Many factors have been studied by researchers regarding the strength of the bond between the concrete surface and the FRP such as using anchoring system. The existing literature reports potential use of CFRP strips in strengthening the RC rectangular beams, but not on the beams with anchorage to the best knowledge of the authors. There are limited works on shear strengthening of RC beams using mechanically anchored FRP sheets (Lee et al. [25], Mofidi [26], and Mofidi et al. [27]).

Anchorage devices are useful tools to prevent, delay or shift this mode of failure to a less critical one; therefore, it improves the performance of the conventional FRP-strengthening method. The purpose of this study was to determine an effective technique for mechanical anchoring of reinforced concrete beams strengthened using FRP composites. A comprehensive review of existing literature was conducted to explore research findings related to debonding failure mechanisms and anchorage schemes for reinforced concrete structural elements with special attention to mechanical anchorage schemes. Based on the analysis of the data from the literature review, new anchoring technique was proposed. Based on the critical review of the existing literature. The main objectives of this study are to predict the shear strength of RC beams with different anchoring strengthened externally with CFRP composite using Nonlinear Finite Element Analysis (NLFEA) taking into account the effects of four major strengthening configurations in addition to control beam (without CFRP external strengthening) including: 1) RC beams with a depth of 225 mm strengthened externally with 90° U-wrap strip at a spacing of 100 mm without anchoring; 2) RC beams with a depth of 225 mm strengthened externally with 90° U-wrap strip at a spacing of 100 mm with 25 mm CFRP top strips anchoring; 3) RC beams with a depth of 225 mm strengthened externally with 90° U-wrap strip at a spacing of 100 mm with 50 mm CFRP top strips anchoring; and 4) RC beams with a depth of 225 mm strengthened externally with 90° U-wrap strip at a spacing of 100 mm with 75 mm CFRP top strips anchoring. As a result, five models have been constructed and subjected to four points loading. For this purpose, validation of the previous experimental study reported by Shbeeb et al. [28] is firstly simulated using ANSYS software. After that, a parametric study is extended for strengthened RC beams using different beam depth.

2. Methods

Nonlinear Finite Element analysis (NLFEA) is an important and effective tool in the analysis of complex structures. The main benefits that NLFEA provided include: 1) substantial savings in the cost, time, and effort compared with the fabrication and experimental testing of structure elements; 2) allows to change any parameter of interest to evaluate its influence on the structure, such as the compressive strength of concrete; 3) allows us to see the stress, strain, and displacement values at any location and at any load level; 4) the ability to change any parameter of interest, and the capability of demonstrating any interesting behavior at any load value and at any location in the system. Six full-scale models strengthened using CFRP are developed to carry out different investigated parameters.

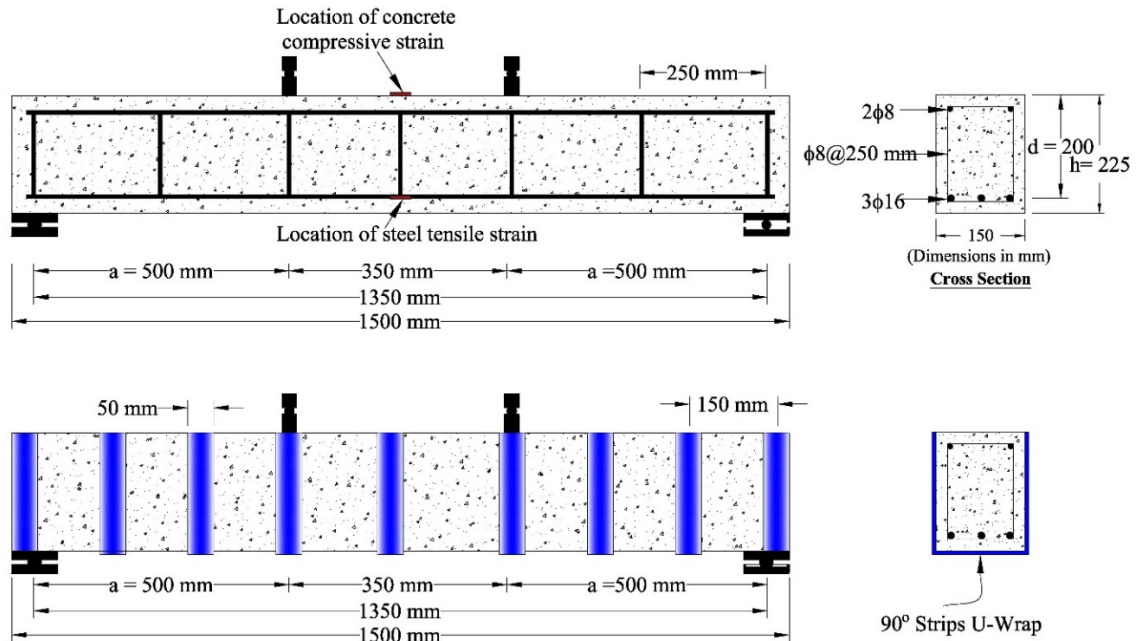


Figure 1. Setup and reinforcement details of the beams [28].

2.1. Experimental Work Review

The validation process of the finite element model is based on the experimental work performed by Shbeeb et al. [28]. High strength reinforced concrete (RC) beams ($150 \times 225 \times 1500$ mm) were designed with shear reinforcement of $\phi 8$ at 250 mm center to center along the entire beam length for all specimens as shown in Fig. 1. Twenty-two rectangular reinforced concrete beams, 150×225 mm with a total length of 1500 mm, were cast with the reinforcement of $2\phi 8$ bars at the top and $3\phi 15$ bars at the bottom. The design choices were made to ensure that shear failure would occur in the beams. Four beams were tested as control beams without strengthening and twenty-four beams were strengthened with different schemes with CFRP strips and sheets. Fig. 1 shows the reinforcement and the CFRP sheet and strips configurations for all the beams specimens. All specimens were tested as simply supported in a special designed built-up rigid steel frame. A hydraulic jack was used to apply a concentrated load through a hydraulic cylinder on a spread steel beam to produce two-point loading condition to generate a constant moment region at mid-span.

2.2. Description of Non-linear Finite Element Analysis (NLFEA)

Concrete is a quasi-brittle material and has different behavior in compression and tension. SOLID65 element is capable of predicting the nonlinear behavior of concrete materials using a smeared crack approach. The model is capable of predicting failure for concrete materials and accounts for both cracking and crushing failures. The two input strength parameters, ultimate uniaxial tensile and compressive strengths, are needed to define a failure surface for the concrete. Consequently, a criterion for failure of the concrete due to a multiaxial stress state can be calculated. Poisson's ratio of 0.2 was used for all beams. The shear transfer coefficient (β_t) represented conditions of the crack face. The value of β_t ranges from 0.0 to 1.0, with 0.0 representing a smooth crack (complete loss of shear transfer) and 1.0 representing a rough crack (no loss of shear transfer). The value of β_t was used in many studies of reinforced concrete structures; however, it varied between 0.05 and 0.25. Therefore, a value of 0.2 for β_t was used in this study. The concrete properties include concrete compressive strength of 55 MPa, initial Young's modulus (E_c) of 35063 MPa. In tension, the stress-strain curve for concrete is assumed to be linearly elastic up to the

ultimate tensile strength. After this point, the concrete cracks and the strength decreases to zero. Fig. 2 shows the stress-strain relationships that are used in this study. The steel for the finite element models was assumed to be an elastic-perfectly plastic material identical in tension and compression.

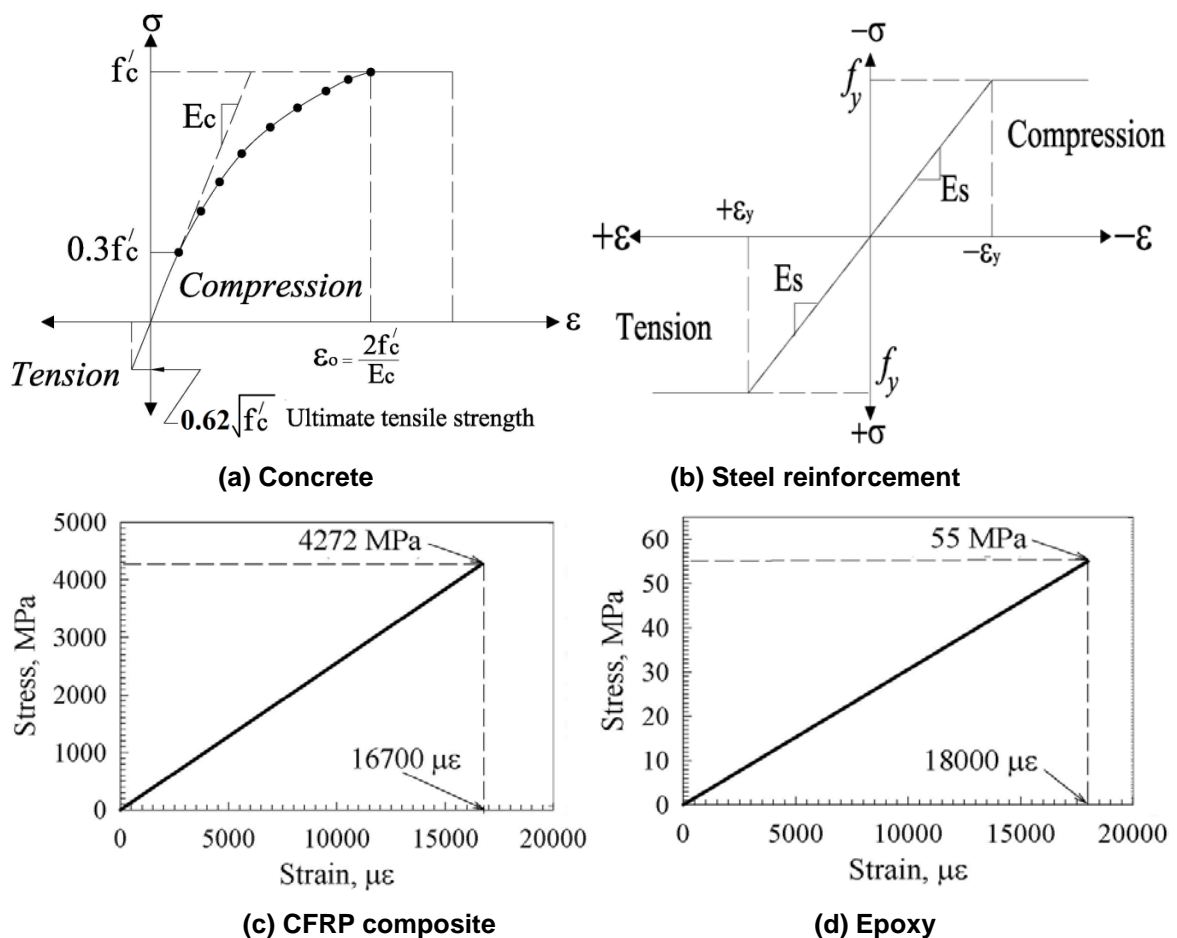


Figure 2. Stress-strain curves [28].

Good results were attained upon utilizing the 3D LINK180 uniaxial tension-compression spar in the simulation of the steel reinforcement, separately, to make it possible to predict: the impact of plasticity, huge and rotational stains, and deflections. Poisson's ratio and yield stress of 0.3 and 413 MPa (Grade 60) respectively were used for the steel reinforcement. Fig. 2(b) shows the stress-strain relationship. Steel plates were added at both ends of the beams to provide a more even stress distribution over the support areas. The steel plates were assumed to be linear elastic materials with an elastic modulus equal to 200 GPa and Poisson's ratio of 0.3. The CFRP composite and epoxy are modeled by a layered solid element, SOLID46. The CFRP is assumed to be an orthotropic material of 0.165 mm thick, tensile strength of 3790 MPa, elastic modulus of 228 GPa, and ultimate tensile strain of 0.017 mm/mm. The epoxy used is 0.343 mm thick, ultimate tensile strength was 55 MPa, elastic modulus was 30 GPa, and ultimate tensile strain was 1800 $\mu\epsilon$. In the other directions perpendicular to the fiber direction, the elastic modulus of CFRP was assumed to be 10^{-6} times that of the main direction. Linear elastic properties were assumed for both CFRP composites and epoxy.

The total load applied was divided into a series of load increments or load steps. Newton-Raphson equilibrium iterations provide convergence at the end of each load increment within tolerance limits equal to 0.001. Load step sizes were automated by ANSYS program for the maximum and minimum load step sizes. In a concrete element, cracking occurs when the principal tensile stress in any direction lies outside the failure surface. After cracking, the elastic modulus of the concrete element is set to zero in the direction parallel to the principal tensile stress direction. Crushing occurs when all principal stresses are compressive and lies outside the failure surface; subsequently, the elastic modulus is set to zero in all directions, and the element effectively disappears. The finite element model fails impulsively when the crushing capability of the concrete is turned on. Crushing of the concrete started to develop in elements located directly under the loads. Afterwards, adjacent concrete elements crushed within several load steps as well, significantly reducing the local stiffness. Finally, the model showed a large displacement, and the solution diverged. Therefore, the crushing capability was turned off and cracking of the concrete controlled the failure of the finite element models. During concrete cracking and ultimate load stages in which a large number of cracks

appeared, the loads were applied gradually with smaller load increments. Failure for each model was identified when the solution for 0.0045 kN load increment was not converging.

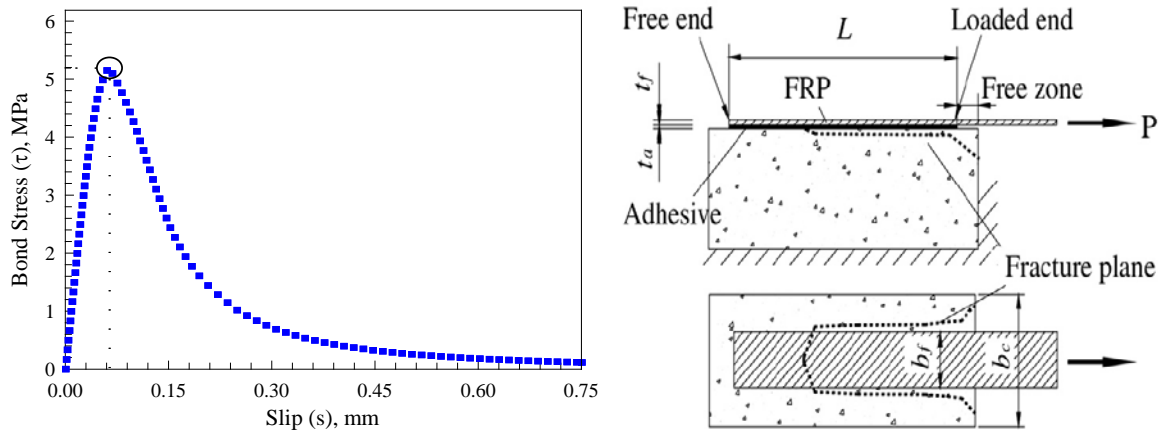


Figure 3. CFRP to concrete bond slip model [29].

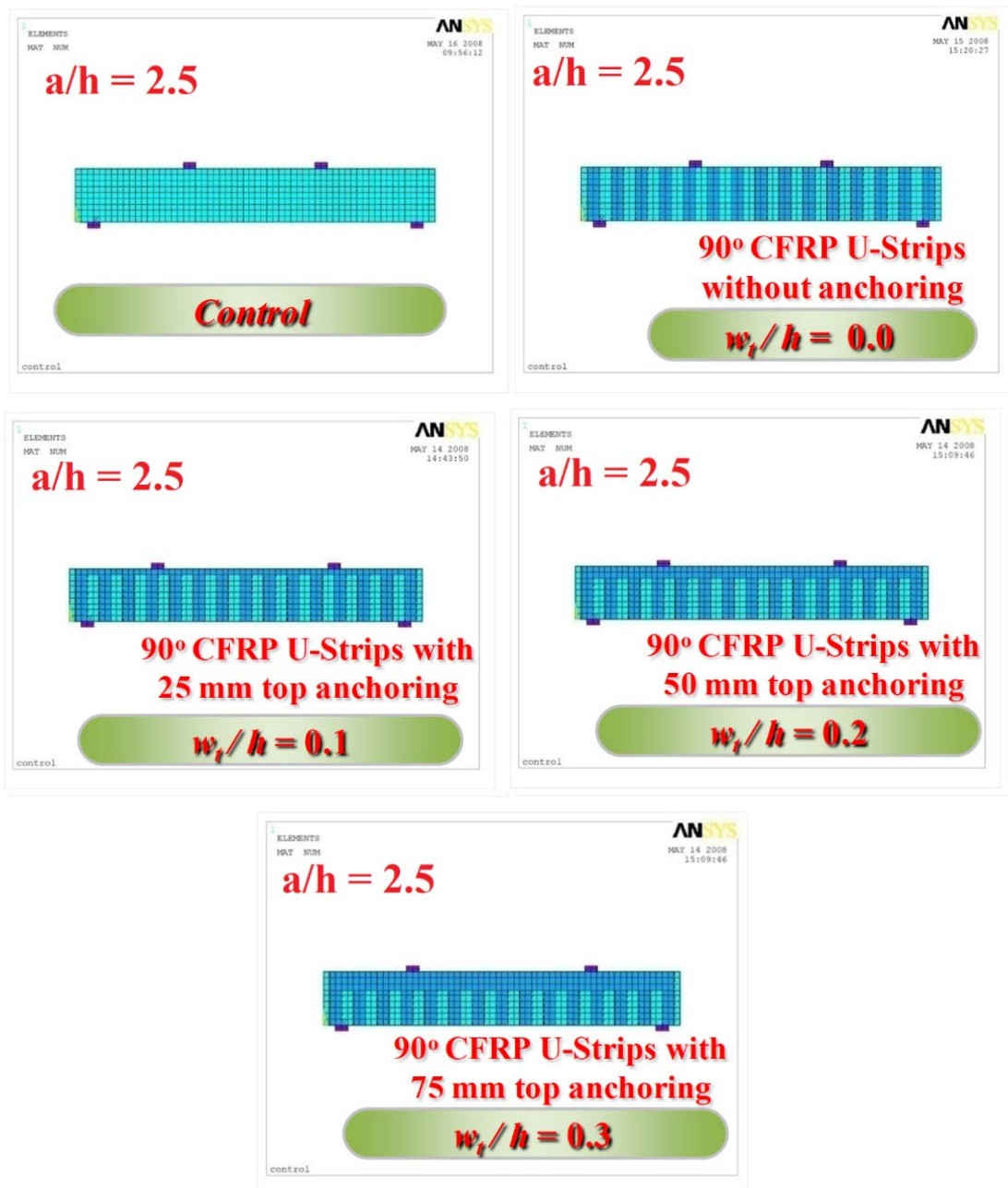


Figure 4. Typical finite element meshing of the beams.

CONTA174 element was used to model the layer between the concrete and epoxy layer. This element is an 8-node element that is intended for general rigid-flexible and flexible-flexible contact analysis. In a general contact analysis, the area of contact between two (or more) bodies is generally not known in advance. Also, CONTA174 element is applicable to 3-D geometries. It may be applied for contact between solid bodies or shells. One of the most accurate bond stress slip models that can be incorporated into a finite element analysis is that proposed by Lu et al. [29]. The mechanical behavior of the FRP/concrete interface is represented by a relationship between the local shear stress (τ) and the relative displacement (s), between the FRP composites and the concrete. Three different bond slip relations have been suggested by these authors; these are classified according to their level of sophistication and are referred to as the precise, the simplified, and the bilinear models. In the current study, the simplified model, as shown in Fig. 3, is adopted for its simplicity.

Square and rectangular elements were created for the rectangular volumes (concrete, CFRP, epoxy, and steel plates) using the volume-mapped command. This properly sets the width and length of the steel reinforcement elements to be consistent with the elements and nodes of the concrete. A convergence study was carried out to determine the appropriate mesh density as shown in Fig. 4 in which (a/d) represents the shear span to beam effective depth ratio and (w_r/h) represents the width of the anchored CFRP to the total depth of the beam. The meshing of the reinforcement was a special case and the individual elements were created in the modeling process. However, the necessary mesh attributes for the concrete were set before each section of the reinforcement was created. SOLID46 elements for epoxy and CFRP layers had the same meshing as SOLID65 elements for concrete to allocate the node over the node of each element. The command merge item was used to merge separate entities that have the same location into single entities. To ensure proper modeling, displacement boundary conditions were applied at the planes of symmetry. The symmetry boundary conditions were set first. Nodes defining a plane through the beam cross section at the center of the beam define one plane of symmetry. The support was modeled as a roller and hinge that allows the beam to rotate at the support. The force was applied across the entire centerline of the steel plate. The beams were analyzed simulating 4-point loading case, the distance between the 2-point of loading is 550 mm. The total applied load was divided into a series of small load increments, each 0.45 kN, and the Modified Newton–Raphson equilibrium iterations were used to check the convergence at the end of each load increment within a tolerance value of 0.001. The static analysis type was utilized to obtain the behavior of the beams. The model failure was identified when the solution of 0.0045 kN load increment was not converging.

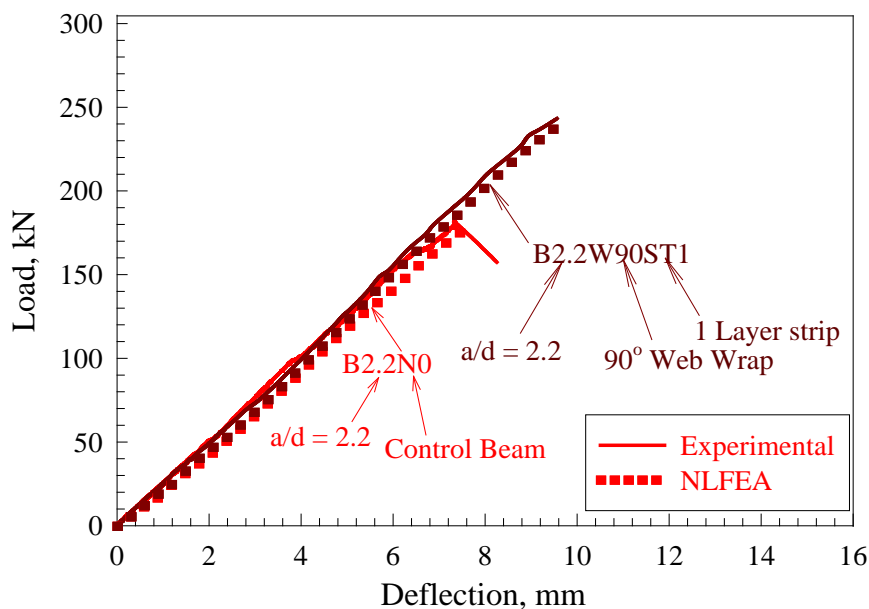


Figure 5. Experimental [28] and NLFEA load-deflection curves.

2.3. Validation Process

Fig. 5 shows the load deflection behavior of experimental and NLFEA results. Inspection of Fig. 5 in terms of pre-cracking stage, after-cracking stage, post-cracking stage, and at failure reveals that the load deflection curves for strengthened beams consist of pre-cracking straight segment followed by a change in slope of the curves after beams cracked at almost 100 kN, which is called “after-cracking”. With further load increase, the beams strengthened with web CFRP strips or sheet failed in shear due to debonding of CFRP

strips or sheet before reaching ultimate flexural capacity. The values of the ultimate strengths and the corresponding percentage increase in the ultimate shear strength of the strengthened beams over the control beam indicated that the performance of the shear deficient beams is enhanced due to the use of CFRP composites. Fig. 5 shows that the NLFEA results correlates well with the experimental data at ultimate load capacity. Fig. 6 shows typical stress contours of the control and strengthened beams.

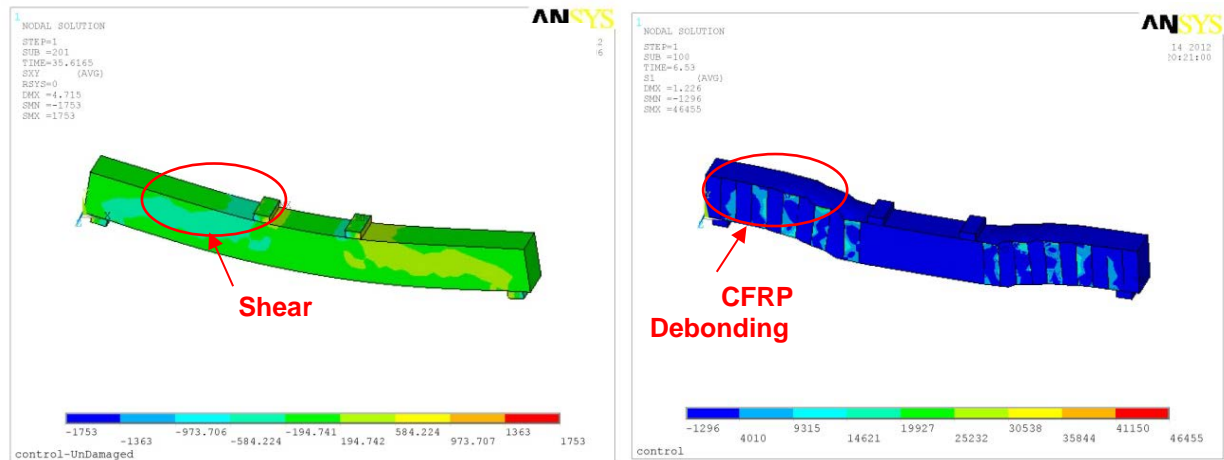


Figure 6. Typical NLFEA stress contours of NLFEA beams.

3. Results and Discussion

3.1. Failure Mode

Fig. 7 shows the representative cracking pattern of B2.7N0. The initial flexural crack of control beam without reinforcement started at the center of the beam within the constant moment region at 23.1 kN. Beyond this load, cracks extended toward the top fiber, and additional flexural cracks developed throughout the beam length. At 77 kN, a 33-degree angle shear crack developed independently of the existing flexural cracks in the center of the shear span. With further load increase, the cracks extended both towards the support and the load point, leading to a sudden, brittle shear failure at 127.3 kN as shown in Fig. 7 and Table 1.

Fig. 7 shows the representative cracking pattern of B2.7U90STA0. The initial flexural crack started at the center of the beam within the constant moment region at 34.2 kN. Beyond this load, cracks extended toward the top fiber, and additional flexural cracks developed throughout the beam length. At 112.5 kN, a 37-degree angle shear crack developed independently of the existing flexural cracks in the center of the shear span. With further load increase, the strip No. 4 debonded at 139.2 kN followed by the debonding of strip No.3 at 142.8 kN. The beam failed successively at 146.0 kN after the debonding of strip No. 5 as shown in Fig. 7 and Table 1. Debonding of the CFRP strip is a delamination between the strip-adhesive-concrete at the strip-end region of the strengthened beam. This failure was a result of the maximum stresses in the adhesive being not greater than the bonding strength between strip-adhesive-concrete at the strip-end region.

Fig. 7 shows the representative cracking pattern of B2.7U90STA1. The initial flexural cracks started at the center of the beam within the constant moment region at 34.2 kN. Beyond this load, cracks extended toward the top fiber, and additional flexural cracks developed throughout the beam length. At 112.1 kN, a 37-degree angle shear crack developed independently of the existing flexural cracks in the center of the shear span. With further load increase, Strip No. 4 debonded at 34 kip followed by the debonding of Strip No. 3 at 161.5 kN. The beam failed successively in shear at 154.4 kN after the debonding of top anchoring strip over Strip No. 3, 4, and 5, respectively, as shown in Fig. 7 and Table 1.

Fig. 7 shows the representative cracking pattern of B2.7U90STA2. The initial flexural crack started at the center of the beam within the constant moment region at 33.8 kN. Beyond this load, cracks extended toward the top fiber, and additional flexural cracks developed throughout the beam length. At 115.6 kN, a 37-degree angle shear crack developed independently of the existing flexural cracks in the center of the shear span. With further load increase, Strip No. 4 debonded at 124.5 kN followed by the debonding of Strip No. 3 at 140.1 kN. The beam failed successively in shear at 163.3 kN after the debonding of top anchoring strip over Strip No. 3 and 4, respectively, as shown in Fig. 7 and Table 1.

Fig. 7 shows the representative cracking pattern of B2.7U90STA3. The initial flexural crack started at the center of the beam within the constant moment region at 34.2 kN. Beyond this load, cracks extended toward the top fiber, and additional flexural cracks developed throughout the beam length. At 112.5 kN, a

37-degree angle shear crack developed independently of the existing flexural cracks in the center of the shear span. With further load increase, Strip No. 4 debonded at 169.0 kN followed by the debonding of Strip No. 3 at 169.9 kN. The beam failed successively in flexure at 170.9 kN after the debonding of top anchoring strip over Strip No. 3 and 4, respectively, as shown in Fig. 7 and Table 1.

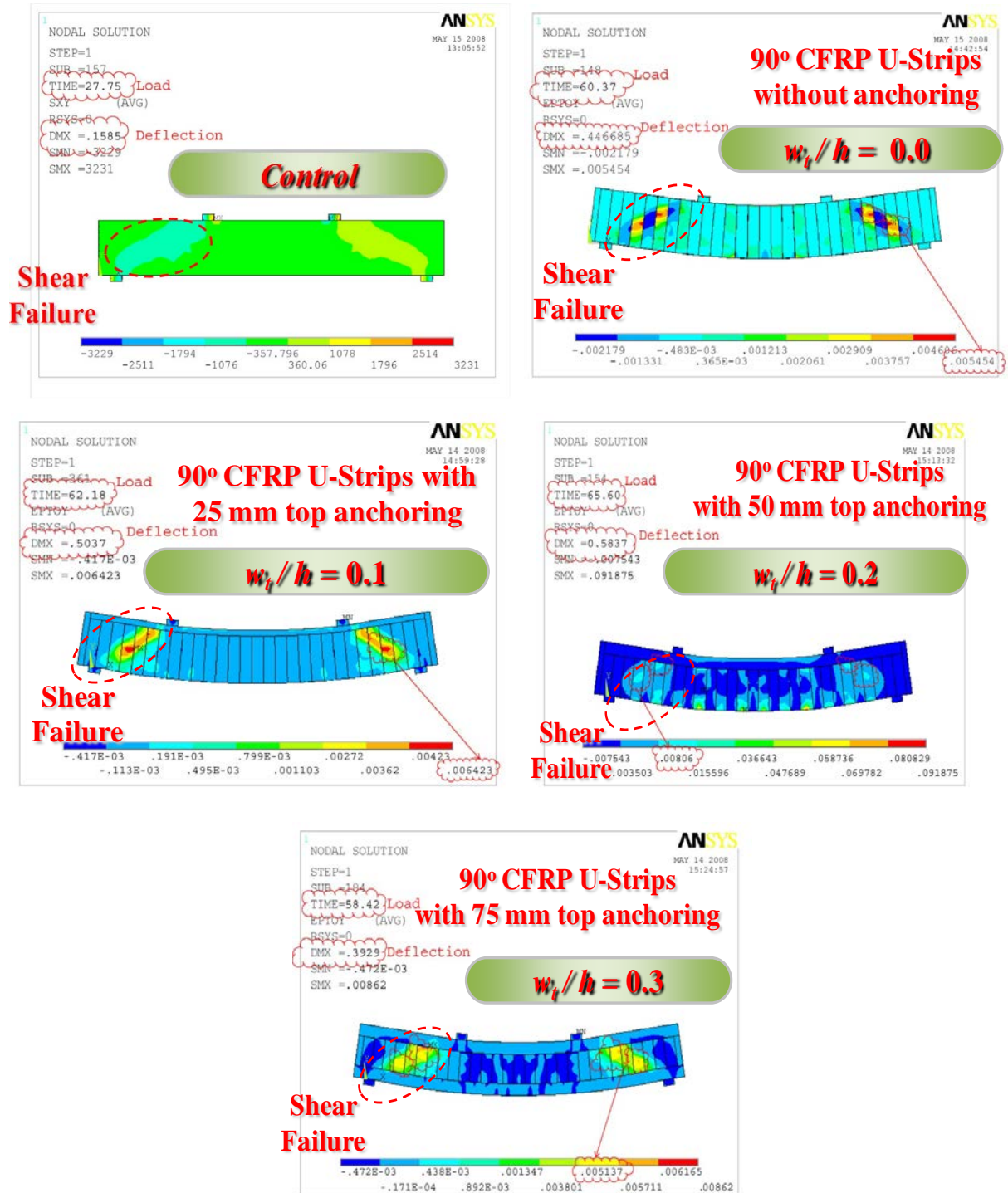
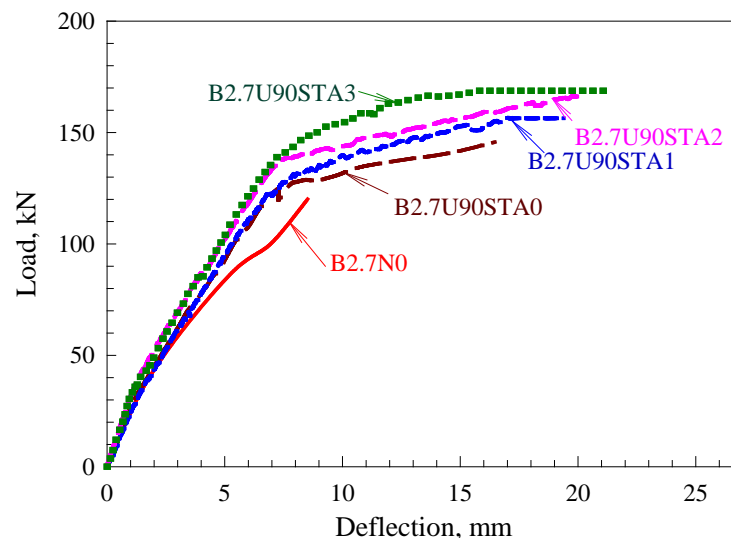


Figure 7. Typical NLFEA stress contours of control NLFEA beams.

Table 1. The details, ultimate load and mode of failure of NLFEA shear beams.

Beam Designation	Type of Strengthening	Ultimate load, kN	Percentage of increase w.r.t control beam, %	Failure mode
B2.7N0	None	127.3	0	Shear failure followed by 33° diagonal crack
B2.7U90STA0	Strip@ 90° U-wrap without anchoring	146.0	15	Shear failure followed by 37° diagonal crack, debonding of CFRP strips
B2.7U90STA1	Strip@ 90° U-wrap with 25 mm CFRP top strips anchoring	154.4	21	Shear failure followed by 37° diagonal crack, debonding of CFRP strips
B2.7U90STA2	Strip@ 90° U-wrap with 50 mm CFRP top strips anchoring	163.5	28	Shear failure followed by 37° diagonal crack, debonding of CFRP strips
B2.7U90STA3	Strip@ 90° U-wrap with 75 mm CFRP top strips anchoring	170.9	34	Flexural failure followed by crushing of concrete in compression zone

**Figure 8. NLFEA load-deflection curves.**

3.2. Load-deflection behavior

Fig. 8 shows the load deflection curves for B2.7N0, B2.7U90STA0, B2.7U90STA1, B2.7U90STA2, and B2.7U90STA3. All strengthened beams exhibited almost linear load deflection relationships up to the load of 133.0 kN that equals the failure load of control beam. This indicates that the CFRP started to carry the load after the formation of the diagonal shear. Inspection of Figure 8 shows that the ultimate load capacity of the beams increased with the increase of anchoring system width, while an increase in stiffness can be observed from the rotation angle of the elastic stage curve of the NLFEA beams. In addition, Fig. 8 shows that the ductility of the beam increased with the increase of anchoring system width exactly mirroring the mode of failure.

3.3. Concrete compressive strain

Fig. 9 exhibits the concrete's compressive strain's (Fig. 1) relationship with the applied load for: B2.7N0, B2.7U90STA0, B2.7U90STA1, B2.7U90STA2, and B2.7U90STA3. When the load was raised, the concrete's compression strain enhanced. In the beams: B2.7N0, B2.7U90STA0, B2.7U90STA1, B2.7U90STA2, and B2.7U90STA3, the load values corresponding to a compressive strain of 1150 $\mu\epsilon$, were 118.3, 128.5, 130.3, 140.6, and 141.5 kN, respectively. This indicates that the more the width of the anchorage, the less the concrete's compressive strain. The largest level of strain was observed in the B2.2W45ST1 beam, which was strengthened with sheets of CFRP. Furthermore, the load-compressive

strain curves of the beams in the second group, the concrete in the beam B2.7U90STA3 had a strain higher than $3000 \mu\epsilon$.

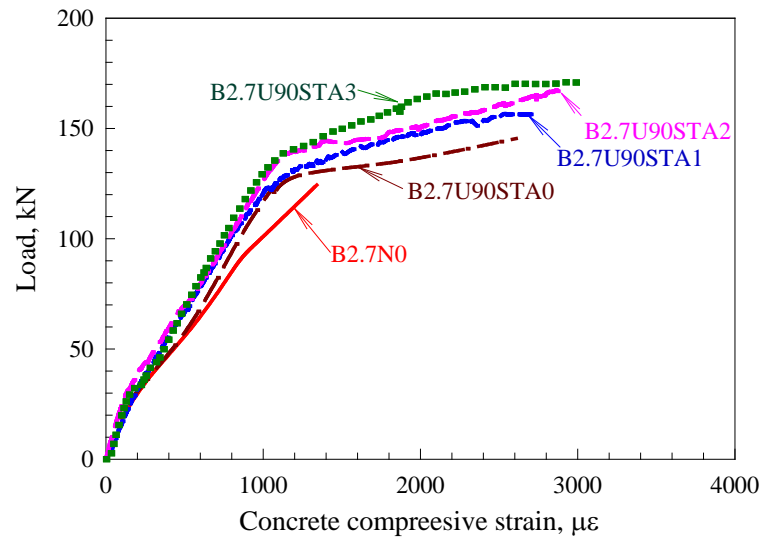


Figure 9. NLFEA load-concrete compressive strain curves.

3.4. CFRP tensile strain

Fig. 10 shows the relationship between the load and CFRP sheet tensile strain for B2.7U90STA0, B2.7U90STA1, B2.7U90STA2, and B2.7U90STA3 RC beams. According to Fig. 6, the tension strain was initiated in the CFRP sheet after the diagonal shear crack started to form at loads of 77.0, 85.8, 85.2, 87.6, and 90.3 kN for B2.7N0, B2.7U90STA0, B2.7U90STA1, B2.7U90STA2, and B2.7U90STA3 beams, respectively. Fig. 10 also shows that the development of strains becomes sluggish around a load of 93.4 kN in all beams. Inspection of Fig. 10 reveals that the CFRP tensile sheet strain increased with the increase in the width of the anchorage system. From this, it is known that the development of strain gets slower as the anchoring system width decreases. At ultimate load, the tensile strains were $3165 \mu\epsilon$, $5960 \mu\epsilon$, $8230 \mu\epsilon$, and $11800 \mu\epsilon$ for B2.7U90STA0, B2.7U90STA1, B2.7U90STA2, and B2.7U90STA3 beams, respectively, which is equivalent to $0.19 \epsilon_{fu}$, $0.35 \epsilon_{fu}$, $0.48 \epsilon_{fu}$, and $0.69 \epsilon_{fu}$, respectively. These higher strains of CFRP strips reflected the efficiency of the anchorage system in the strengthening of shear deficient beams. Therefore, the B2.7U90STA3 strengthened beam showed higher tensile strain than other strengthened beams for the same load.

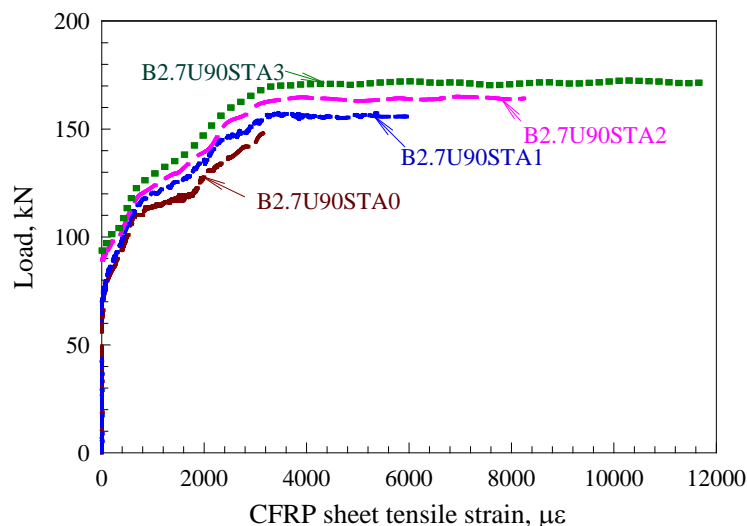


Figure 10. NLFEA load- CFRP tensile strain curves.

3.5. Steel tensile strain

Fig. 11 shows the relationship between the load and strain at the level of steel (Fig. 1) for B2.7N0, B2.7U90STA0, B2.7U90STA1, B2.7U90STA2, and B2.7U90STA3 RC beams. The load strain curve followed the same trend for all the beams before the cracking. After cracking, the slope of the curve was

reduced as a result of reduction in stiffness. Inspection of Fig. 11 reveals that the steel tensile strain followed the same trend and behavior as the concrete compressive strain which increased with increasing the load, while the steel tensile strain in the concrete decreased with the increase in the width of the anchoring system. All the anchored beams reached the yielding point, while the steel reinforcement in B2.7U90STA3 strengthened beam experienced the highest tensile strain development among other beams at ultimate load.

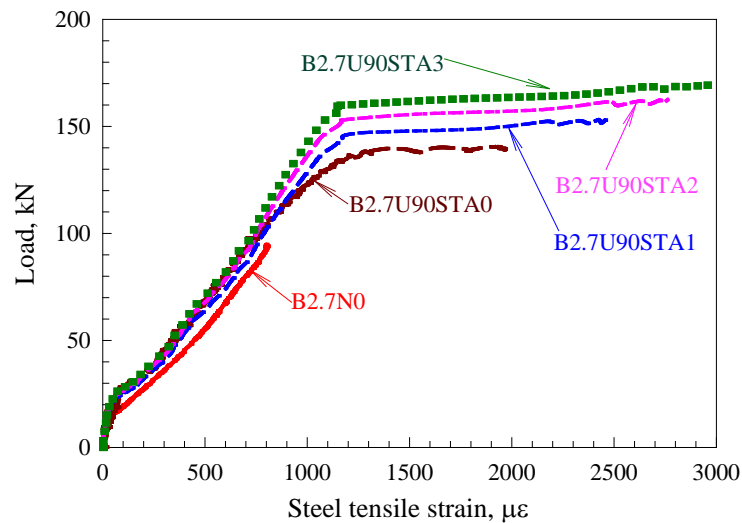


Figure 11. NLFEA load-steel tensile strain curves.

3.6. Crack opening behavior

Fig. 12 shows the relationship between the load and crack opening for B2.7N0, B2.7U90STA0, B2.7U90STA1, B2.7U90STA2, and B2.7U90STA3 RC beams. According to Fig. 8, crack began opening after the diagonal shear its initiation at load 77.0, 85.8, 85.2, 87.6, and 90.3 kN for B2.7N0, B2.7U90STA0, B2.7U90STA1, B2.7U90STA2, and B2.7U90STA3, respectively, after diagonal shear crack formed. Fig. 12 shows that the development of crack width becomes sluggish around 0.25 mm in all beams as well. It can be observed the crack developed at a slower rate as the anchoring system width increased. At ultimate load, the ultimate crack width is 1.78, 1.19, 1.12, 1.03, and 0.81 mm for B2.7N0, B2.7U90STA0, B2.7U90STA1, B2.7U90STA2, and B2.7U90STA3, respectively. Therefore, the B2.7U90STA3 strengthened beam showed less crack width for the same load than the other beams.

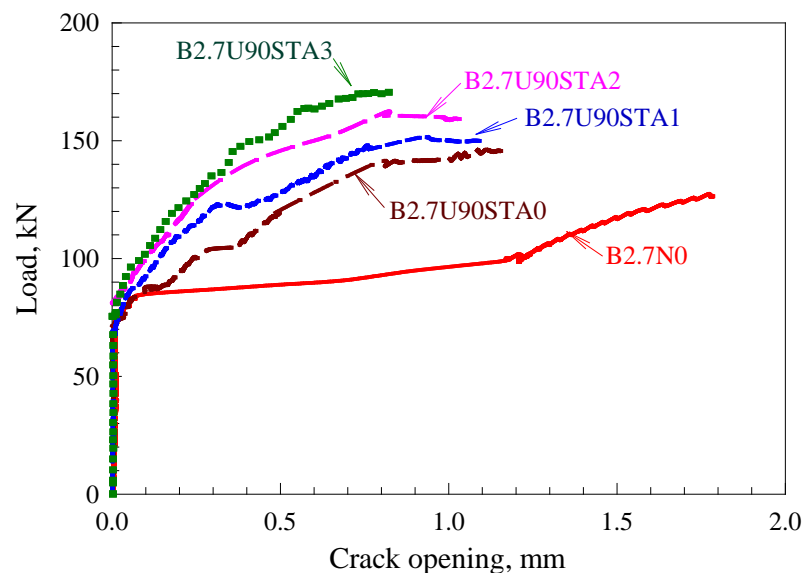


Figure 12. NLFEA load-crack opening curves.

3.7. Comparison of NLFEA with theoretical models

For purposes of comparison, the predictions of the NLFEA results are compared with those of the ACI model [30], Triantafillou model [31], and Colotti et al. model [32]. In the ACI, Triantafillou, and Colotti et al. models, the general design guidance is clearly derived from the experimental data and they are only

applicable to external FRP reinforcement. Fig. 13 shows a comparison of the results predicted by the three models $V_{f,NLFEA}/V_{f,ACI}$ [30], $V_{f,NLFEA}/V_{f,Tri}$ [31], and $V_{f,NLFEA}/V_{f,Col}$ [32]. Note that the ACI and Triantafillou models were calibrated for CFRP and should be used with caution for other types of composites as shown in Fig. 13. The overall predictions by ACI model appear to be overestimated with a mean $V_{f,NLFEA}/V_{f,ACI}$ value of 1.32 and a coefficient of variation (COV) of 25 %, while the NLFEA results for Colotti et al. model are underestimated with a mean $V_{f,NLFEA}/V_{f,Col}$ value of 0.70 and a COV of 20 %. However, Triantafillou et al. model shows a weak agreement with NLFEA results, with a mean $V_{f,NLFEA}/V_{f,Tri}$ value of 0.5 and (COV) of 18 %. It is also important to take into consideration that all the ACI and Triantafillou models are semi empirical in nature, with important governing parameters derived from test data for beams strengthened with FRP laminates, whereas the ACI model cannot be applied in certain cases. In addition, a careful inspection of Fig. 13 will show that the ACI model has a much wider range of NLFEA/theoretical failure load ratios of 0.95 to 1.74. The Triantafillou model also gives a non-acceptable range of NLFEA/theoretical mean values of 0.41 to 0.59. On the contrary, the Colotti et al. model gives a much larger range of NLFEA/theoretical mean values of 0.53 to 0.88 than Triantafillou model.

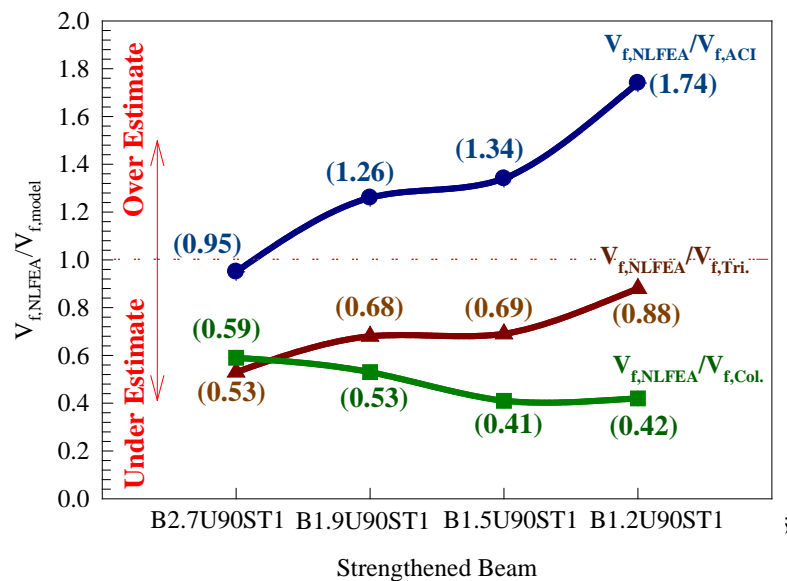


Figure 13. The normalized NLFEA FRP shear force with respect to analytical models.

4. Conclusions

1. The use of CFRP composites is an effective technique to enhance the shear capacity of RC beams. The externally bonded CFRP can increase the shear capacity of the beam significantly by 15–34 % compared to that of the control beams, depending on the variables investigated.
2. One of the observed failure modes was debonding of more than two CFRP strips. Test results seem to indicate that this mechanism can be prevented by providing CFRP strips anchorage in the beam from top side.
3. Bonded anchorage of CFRP strips with width of 0.1h, 0.2h, and 0.3h to the beam caused a decrease in average interface bond stress and an increase in the effective strain of the CFRP sheet at failure, which resulted in a higher shear capacity as compared with that of the U-wrapped beams without anchorage as well as helped delay or mitigate the sheet debonding from the concrete surface.
4. The inclination of the primary shear crack influenced the shear strength contribution of the external strengthening. As this study demonstrated, the shear crack angle determined the number of CFRP strips intersected by the crack and whether or not an intersected CFRP strip was fully effective.
5. The overall predictions by ACI model [30] appear to be overestimated with a mean value of 1.32 and a coefficient of variation (COV) of 25 % and underestimated in the NLFEA results for Colotti et al. model with a mean value of 0.70 and a COV of 20 %. However, Triantafillou et al. model shows a weak agreement with NLFEA results.

References

1. Ahmed, A., Kodur, V. The experimental behavior of FRP-strengthened RC beams subjected to design fire exposure. Engineering Structures. 2011. 33(1). Pp. 2201–2211. DOI: 10.1016/j.engstruct.2011.03.010

2. Mabsout, M., Tarhini, K., Jabakhanji, R., Awwad, E. Wheel load distribution in simply supported concrete slab bridges. *J Bridge Eng.* 2004. 9(2). Pp. 293–306. DOI: 10.1061/(ASCE)1084-0702(2004)9:2(147)
3. Al-Rousan, R., Abo-Msamh, I. Bending and Torsion Behaviour of CFRP Strengthened RC Beams. *Magazine of Civil Engineering.* 2019. 92(8). Pp. 62–71. DOI: 10.18720/MCE.92.8
4. Al-Rousan, R. Behavior of two-way slabs subjected to drop-weight. *Magazine of Civil Engineering.* 2019. 90(6). Pp. 62–71. DOI: 10.18720/MCE.90.6
5. Al-Rousan, R. The impact of cable spacing on the behavior of cable-stayed bridges. *Magazine of Civil Engineering.* 2019. 91(7). Pp. 49–59. DOI: 10.18720/MCE.91.5
6. Yu, B., Kodur, V.K.R. Fire behavior of concrete T-beams strengthened with nearsurface mounted FRP reinforcement. *Engineering Structures.* 2014. 80(1). Pp. 350–361. DOI: 10.1016/j.engstruct.2014.09.003
7. Triantafyllou, T.C., Antonopoulos, C.P. Design of concrete flexural members strengthened in shear with FRP. *J Compos Constr.* 2000. 4(4). Pp.198–205. DOI: 10.1061/(ASCE)1090-0268(2000)4:4(198)
8. Boussselham, A., Chaallal, O. Shear strengthening reinforced concrete beams with fiber-reinforced polymer: assessment of influencing parameters and required research. *ACI Struct J.* 2004. 101(2). Pp. 219–227. DOI: 10.14359/13019
9. Belarbi, A., Bae, S., Brancaccio, A. Behavior of full-scale RC T-beams strengthened in shear with externally bonded FRP sheets. *Constr Build Mater.* 2012. 32 (1). Pp. 27–40. DOI: 10.1016/j.conbuildmat.2010.11.102
10. Khalifa, A., Nanni, A. Improving shear capacity of existing RC T-section beams using CFRP composites. *Cem Concr Compos.* 2000. 22 (1). Pp. 165–174. DOI: 10.1016/S0958-9465(99)00051-7
11. Mosallam, A., Banerjee, S. Shear enhancement of reinforced concrete beams strengthened with FRP composite laminates. *Composites: Part B.* 2007. 38 (1). Pp. 781–93. DOI: 10.1016/j.compositesb.2006.10.002
12. Ashrafuddin, M., Baluch, M.H., Sharif, A., Al-Sulaimani, G.J., Azad, A.K., Khan, A. Peeling and diagonal tension failures in steel plated R/C beams. *Constr Build Mater.* 1999. 13 (1). Pp. 459–467. DOI: 10.1016/S0950-0618(99)00044-6
13. Rangan, B.V. Shear design of reinforced concrete beams, slabs and walls. *Cem Concr Compos.* 1998. 20 (1). Pp. 455–464. DOI: 10.1016/S0958-9465(98)00027-4
14. Spadea, G., Bencardino, F., Swamy, R.N. Optimizing the performance characteristics of beams strengthened with bonded CFRP laminates. *Mater Struct.* 2000. 33 (1). Pp. 1119–1126. DOI: 10.1007/BF02484166
15. Malek, A.M., Saadatmanesh, H. Ultimate shear capacity of reinforced concrete beams strengthened with web-bonded fiber-reinforced plastic plates. *ACI Struct J.* 1998. 95 (4). Pp. 391–399. DOI: 10.14359/555
16. Triantafyllou, T.C. Shear strengthening of reinforced concrete beams using epoxy-bonded FRP composites. *ACI Struct J.* 1998. 95 (2). Pp. 107–115. DOI: 10.14359/531
17. Khalifa, A., Nanni, A. Improving shear capacity of existing RC T-section beams using CFRP composites. *J Cem Concr Compos.* 2000. 22 (2). Pp.165–174. DOI: 10.1016/S0958-9465(99)00051-7
18. Hutchinson, R.L., Rizkalla, S.H. Shear strengthening of AASHTO bridge girders using carbon fiber reinforced polymer sheets. *ACI Special Publications (SP-188).* 1999. 188 (1). Pp. 945–958. DOI: 10.14359/5692
19. Zhang, Z., Hsu, C.T. Shear strengthening of reinforced concrete beams using carbon-fiber-reinforced polymer laminates. *J Compos Constr.* 2005. 9 (2). Pp. 158–169. DOI: 10.1061/(ASCE)1090-0268(2005)9:2(158)
20. Monti, G., Liotta, M.A. Tests and design equations for FRP-strengthening in shear. *Constr Build Mater.* 2007. 21 (24). Pp.799–809. DOI: 10.1016/j.conbuildmat.2006.06.023
21. Deniaud, C., Cheng, J.J.R. Shear behaviour of reinforced concrete T-beams with externally bonded fiber-reinforced polymer sheets. *ACI Struct J.* 2001. 98 (3). Pp. 386–394. DOI: 10.14359/10227
22. Boussselham, A., Chaallal, O. Behaviour of reinforced concrete T-beams strengthened in shear with carbon fiber-reinforced polymer—an experimental study. *ACI Struct J.* 2006. 103 (3). Pp. 339–347. DOI: 10.14359/15311
23. Boussselham, A., Chaallal, O. Effect of transverse steel and shear span on the performance of RC beams strengthened in shear with CFRP. *Composites: Part B.* 2006. 37 (1). Pp. 37–46. DOI: 10.1016/j.compositesb.2005.05.012
24. Boussselham, A., Chaallal, O. Mechanisms of Shear Resistance of Concrete Beams strengthened in shear with externally bonded FRP. *J Compos Constr.* 2008. 12 (5). Pp. 499–512. DOI: 10.1061/(ASCE)1090-0268(2008)12:5(499)
25. Lee, H.K., Cheong, S.H., Ha, S.K., Lee, C.G. Behaviour and performance of RC T-section deep beams externally strengthened in shear with CFRP sheets. *J Compos Struct.* 2011. 93 (1). Pp. 911–922. DOI: 10.1016/j.compstruct.2010.07.002
26. Gala, K., Mofidi, A. Shear strengthening of RC T-beams using mechanically- anchored unbonded dry carbon fibre sheets. *ASCE, J Perform Constr Facil.* 2010. 24(1). Pp. 31-39. DOI: 10.1061/(ASCE)CF.1943-5509.0000067
27. Mofidi, A., Chaallal, O., Benmokrane, B., Neale, K. Performance of end-anchorage systems for RC Beams strengthened in shear with epoxy bonded FRP. *J Compos Constr.* 2012. 16 (3). Pp. 322-331. DOI: 10.1061/(ASCE)CC.1943-5614.0000263
28. Shbeeb, N.I., Al-Rousan, R., Issa, M.A., Al-Salman, H. Impact of bonded carbon fibre composite on the shear strength of reinforced concrete beams. *Proceedings of the Institution of Civil Engineers: Structures and Buildings.* 2018. 171 (5). Pp. 364–379. DOI: 10.1680/jstbu.16.00145
29. Lu, X.Z., Teng, J.G., Ye, L.P., Jiang, J.J. Bond-slip models for FRP sheets/plates bonded to concrete. *Engineering Structures Journal* 2005. 27 (1). Pp. 920–937. DOI: 10.1016/j.engstruct.2005.01.014
30. ACI Committee 440. Design and Construction of Externally Bonded FRP Systems for strengthening Concrete Structures. *ACI440.2R-02. 2002. American Concrete Institute, Farmington Hills, Mich.: 45 pp. DOI: 10.1061/40753(171)159. ISBN: 9780870312854
31. Triantafyllou, T.C. Shear strengthening of reinforced concrete beams using epoxy-bonded FRP composites. *ACI Struct J.* 1998. 95 (2). Pp. 107–115. DOI: 10.14359/531
32. Colotti, V., Spadea, G., Swamy, R.N. Structural Model to Predict the Failure Behavior of Plated Reinforced Concrete Beams. *Journal of Composite Construction.* 2004. 8 (2). Pp. 104–122. DOI: 10.1061/(ASCE)1090-0268(2004)8:2(104)

Contact:

Rajai Al-Rousan, rzalrousan@just.edu.jo